Selective conversion of {Mo_{132}} Keplerate ion into 4-electron reduced crown-capped Keggin derivative $[Te_5Mo_{15}O_{57}]^{8-}$. A key intermediate to single phase M1 multielement MoVTeO light alkanes oxidation catalyst.

Romain Canioni,[a] Catherine Marchal-Roch,[a] Nathalie Leclerc-Laronze,[a] Mohamed Haouas,[a] Francis Taulèlle,[a] Arnaud Etcheberry,[a] Sebastien Paul,[b] Carole Lamonier,[b] Jean-François Paul,[b] Stéphane Loridant,[c] Jean-Marc M. Millet,[c] Emmanuel Cadot*[a]

Electronic Supporting Information

Organisation of the ESI section

1. General Procedure

Raman spectra were recorded under microscope with a Labram HR Jobin Yvon-Horiba spectrophotometer, equipped with a CCD detector. A laser Ar-Kr 2018RM (Spectra Physics) (λ = 514.53 nm) was used as excitation source with a power of 1 mW and was focused with a X50 long working distance objective.

Infrared spectra were recorded on an FTIR magna 550 Nicolet spectrophotometer using KBr pressed pellets. Selected IR and Raman spectra of compounds are given in Figures SI.9, SI.10, SI.11 and SI.12.

NMR measurements. ^{1}H NMR spectra were performed on a Bruker Avance 300 spectrometer, operating at 300 MHz in 5 mm tubes. Chemical shifts were referenced to the external TMS standard. ^{125}Te NMR spectra were recorded at 126.479 MHz in H_2O/D_2O using a 10 mm tube on a Bruker Avance 400 instrument. Each spectrum was referenced to an aqueous solution of telluric acid as δ = 713 ppm relative to the primary reference $(CH_3)_2Te$. Controlled-temperature experiments utilized Bruker's Variable Temperature Unit. The probe temperatures were calibrated using the chemical shift differences in the ^{1}H peaks of of ethylene glycol as external standards. Spin-lattice relaxation times (T_1) were determined at room temperature for the various ^{125}Te NMR signals by the saturation recovery method following individual on-resonance saturating cw irradiation.

Elemental analysis was performed by the Service Central d'Analyse, USR-59, CNRS in Vernaison, France. Water content was determined by thermal gravimetric analysis (TGA-7, Perkin-Elmer).

X-ray crystallographic study. A well-shaped dark-blue needle-like crystal (0.40 x 0.10 x 0.10 mm^3) of $Na_{2.5}(NH_4)_{5.5}Te_5Mo_{15}O_{57}\bullet 20H_2O$ (**2b**) was mounted in sealed Lindeman tubes to prevent any loss of crystallization water. Intensity data collections for **2b** were carried out at room temperature on a Siemens SMART-CCD area detector system equipped with a normal-focus molybdenum-target X-ray tube (λ = 0.71073 Å). An empirical absorption correction based on the method of Blessing[1] was applied by using the SADABS program.[2] The structures were solved by direct methods and refined by the full-matrix least squares method by using the SHELX-TL package.[3] Relevant crystallographic data for compounds **2b** are reported in Table S1. Heavier atoms (tellurium and molybdenum) were

Table S1: Selected X-ray crystallographic data for **2b**.

Formula	$\mathbf{Na_{2.5}(NH_4)_{5.5}[TeMo_{15}O_{57}]\bullet 20H_2O}$	ρ_{calc}, g.cm^{-3}	2.899
M, g.mol^{-1}	3543.5	μ(MoKα), Å	4.490
crystal size (mm)	0.40x0.10x0.10	λ(MoKα), Å	0.71073
crystal system	$C_{2/c}$	θ range, deg	1.28-30.36
a, Å	23.835(2)	data collected	56074
b, Å	25.548(2)	unique data	21571
c, Å	26.003(2)	unique data I>2σ(I)	12815
α, deg	90	Parameters number	820
β, deg	110.251(2)	$R_1(F)$[a]	0.0664
γ, deg	90	wR_2 (F^2)	0.1115
V, Å^3	14855(2)	GOF	0.982
Z	2		

$$R_1 = \frac{\Sigma\left|F_O\right| - \left|F_C\right|}{\Sigma\left|F_C\right|} \qquad wR_2 = \sqrt{\frac{\Sigma w(F_O^2 - F_C^2)^2}{\Sigma w(F_O^2)^2}} \qquad \frac{1}{w} = \sigma^2 F_O^2 + (aP)^2 + bP$$

1 R. Blessing, *Acta Crystallogr., Sect. A*., 1995, **51**, 33.
2 G. M. Sheldrick, SADABS; program for scaling and correction of area detector data, University of Göttingen, Germany, 1997.
3 G. M. Sheldrick, *Acta Crystallogr., Sect. A*., 1990, **46**, 467; SHELX-TL, version 5.03, Software Package for Crystal Structure Determination, G. M. Sheldrick, Siemens Analytical X-ray Instrument Division, Madison, WI, 1994.

initially located by direct methods. The remaining non-hydrogen atoms were located from Fourier differences and were refined with anisotropic thermal parameters. The disordered atoms, alkali cations, nitrogen of ammonium or oxygen atoms of crystallized water were isotropically refined. Among the 2.5 Na cations and 5.5 ammonium cations found by elemental analysis, only one sodium atom was located, probably due to severe disorders with water molecules, a common feature for polyoxometalate structures. Further details on the crystal structure investigation may be obtained from the Fachinformationszentrum Karlsruhe, 76344 Eggenstein-Leopoldshafen, Germany (fax: (+49) 7247-808-666; e-mail: crysdata@fiz-karlsruhe. de), on quoting the depository number CSD-422500 for **2b**.

Catalytic data.

The prepared M1 phases were tested for the oxidative dehydrogenation of ethane. The experiments were performed at atmospheric pressure and isothermal conditions using a glass plug-flow micro-reactor glass, 1 g of catalyst and reactant flow of 31.25 mL.min^{-1} (W/F = 40.5) composed of oxygen, ethane and helium with the relative composition 30/20/50. The reaction temperature varied between 360 and 420°C. Ethane, ethylene, CO and CO_2 were analyzed online, using a gas chromatograph equipped with a TCD detector and a Carboxen 1000 column; Ne was used as internal standard. The catalytic data were collected for at least 72 h. No change in catalytic properties was observed during this time.

Table S2: Catalytic performances of the M1 phase $Mo_{8.22}V_{1.78}Te_{0.79}O_{29}\bullet 1H_2O$.

Catalyst	**T(°C)**	**Conversion (%)**	**Selectivity (%)**		
		C_2H_6	CO	CO_2	C_2H_4
M1	400	46	11	6	83

Flow rate: 31.25 mL.min^{-1}; $C_2H_6/O_2/He$ = 20/30/50; W/F = 40.5

2. Synthesis of the compounds

All reagents were used as purchased without further purification. The Keplerate ion $(NH_4)_{42}[Mo_{132}(H_2O)_{72}(CH_3COO)_{30}O_{372}]\bullet 300H_2O\bullet 10CH_3COONH_4$ (abbreviated $\{Mo_{132}\}$ hereafter) was synthesized according to the published procedure [ref. 5(b)].

$(NH_4)_{55.65}Na_3\{[Mo_{132}O_{372}(CH_3COO)_{30}(H_2O)_{72}]_{0.65}(Te_5Mo_{15}O_{57})_3\}\bullet 4CH_3COO\bullet 180H_2O$ (**1**): $\{Mo_{132}\}$ (10g; 0.349 mmol) and Na_2TeO_3 (1.162g; 5.24 mmol) were dissolved in 100 mL of distilled water and the resulting solution was heated up to 70°C under stirring for 60 min. After the mixture was cooled down to room temperature, a light cloudy precipitate was eliminated by filtration and NH_4Cl (9 g; 168 mmol) was added to the resulting filtrate, provoking the precipitation of a dark-brown solid. Then, the solution was cooled in a ice-bath. 60 min later, the brown solid was collected by filtration, washed with ethanol and then dried with diethylether (9.8g; yield: ~100% based on Mo). Elemental analysis (%) calcd for $C_{75.60}H_{691.04}Mo_{132.00}N_{55.65}Na_{3.00}O_{669.18}Te_{14.95}$: C 1.72, Mo 45.97, N 2.83, Na 0.25, Te 6.89; Found: C 1.81, Mo 45.61, N 2.82, Na 0.26, Te 6.91. IR(KBr pellet): 1620(m), 1540(m), 1450(sh), 1400(s), 966(s), 936(sh), 903(vw), 857(m), 794(s), 725(s), 680(sh), 626(w), 569(m), 514(vw), 468(vw), 419(vw) cm^{-1}. Raman (solution): 964(w), 950(w), 882(s), 851(sh),755(vw),714(vw), 374(m), 313(w), 218(vw). The ratio between coordinated and uncoordinated acetate was supported by ^{1}H NMR according to ref. 12.

$Na_{0.4}(NH_4)_{7.6}[Te_5Mo_{15}O_{57}]\bullet 18H_2O\bullet 1.3NH_4Cl$ (**2a**). $\{Mo_{132}\}$ (4.5g; 0.157 mmol) was dissolved in 30 mL of distilled water. The resulting solution is heated up to 70°C. Separately, Na_2TeO_3 (1.533 g; 6.92 mmol) was dissolved in 30 mL of distilled water and then added to the $\{Mo_{132}\}$-containing solution under vigorous stirring. The mixture was left for 120 min at 70°C. The solution was clarified by filtration at 70°C and NH_4Cl (11 g; 210 mmol) was added. The solution was cooled in an ice-bath for 30 min under moderate stirring, allowing the precipitation of a black solid. After filtration, washing and drying with ethanol and diethylether, respectively, 3.8 g of solid was recovered (yield: 78% based on Mo). Elemental analysis (%) calcd for $Cl_{1.3}H_{127.2}Mo_{15}N_{8.9}Na_{0.4}O_{82}Te_5$: Cl 1.26 ,N 3.78, Mo 39.42, Na 0.25, Te 17.38; Found: Cl 1.32, N 3.74, Mo 39.49, Na 0.23, Te 17.46.

$(NH_4)_{5.5}Na_{2.5}[Te_5Mo_{15}O_{57}]\bullet 20H_2O$ (**2b**). Single crystals of the anion $[Te_5Mo_{15}O_{57}]^{8-}$ were obtained through similar procedure described above without the addition of NH_4Cl for precipitation. The filtrate was cooled down at -10°C for 24h. After fusion of the frozen solution, black crystalline needles suitable for X-ray diffraction study were collected by filtration (0.630 g; 13% based on Mo). Elemental analysis (%) calcd for $H_{62}Mo_{15}N_{5.5}Na_{2.5}O_{77}Te_5$: N 2.19, Mo 41.10, Na 1.63, Te 18.12; Found: N 2.08, Mo 40.9, Na 1.63, Te 17.85. IR(KBr pellet): 1620(m), 1400(s), 959(s), 903(m), 781(vw), 719(m), 678(s), 616(m), 561(m), 467(w), 438(w), 428(w) cm^{-1}.

$Mo_{8.22}V_{1.78}Te_{0.79}O_{29}\bullet 1H_2O$ (M1 catalytic phase): compound **1** (1.5 g) and vanadyl sulfate (0.370 g; 1.46 mmol) are suspended in 25 mL of distilled water. The mixture corresponds to the Mo:V:Te:H_2O molar ratio of 1:0.22:0.11:310. The resulting solution was autoclaved in Teflon-lined stainless steel autoclaves at 175 °C for 24 h under stirring. Black crystalline powder (1.0 g) was collected by filtration, washed and dried with ethanol and ether, respectively (yield: 82% based on Mo). Elemental analysis (%) calcd for $Mo_{8.22}V_{1.78}Te_{0.79}O_{29}\bullet 1H_2O$: Mo 53.95, V 6.21, Te 6.87; Found: Mo 53.97, V 6.21, Te 6.88.

3. Potentiometric titration of $Na_{2.5}(NH_4)_{5.5}[Te_5Mo_{15}O_{57}]\bullet 20H_2O$

A potentiometric titration was carried out as follows: $Na_{2.5}(NH_4)_{5.5}[TeMo_{15}O_{57}]\bullet 20H_2O$ (41.3 mg; 1.165 10^{-5} mol) is dissolved in 20 mL of distilled water and 10 mL of 10^{-2} $mol.L^{-1}$ $Ce(SO_4)_2$ aqueous solution. The resulting solution is potentiometrically titrated by a 10^{-2} $mol.L^{-1}$ $FeSO_4$-NH_4SO_4 aqueous solution. A potential jump is observed for 5.30 mL (see Figure S1) which corresponds to a consumption of 4.03 Ce^{4+} (~4 Mo^V) per $[Te_5Mo_{15}O_{57}]^{8-}$ anion.

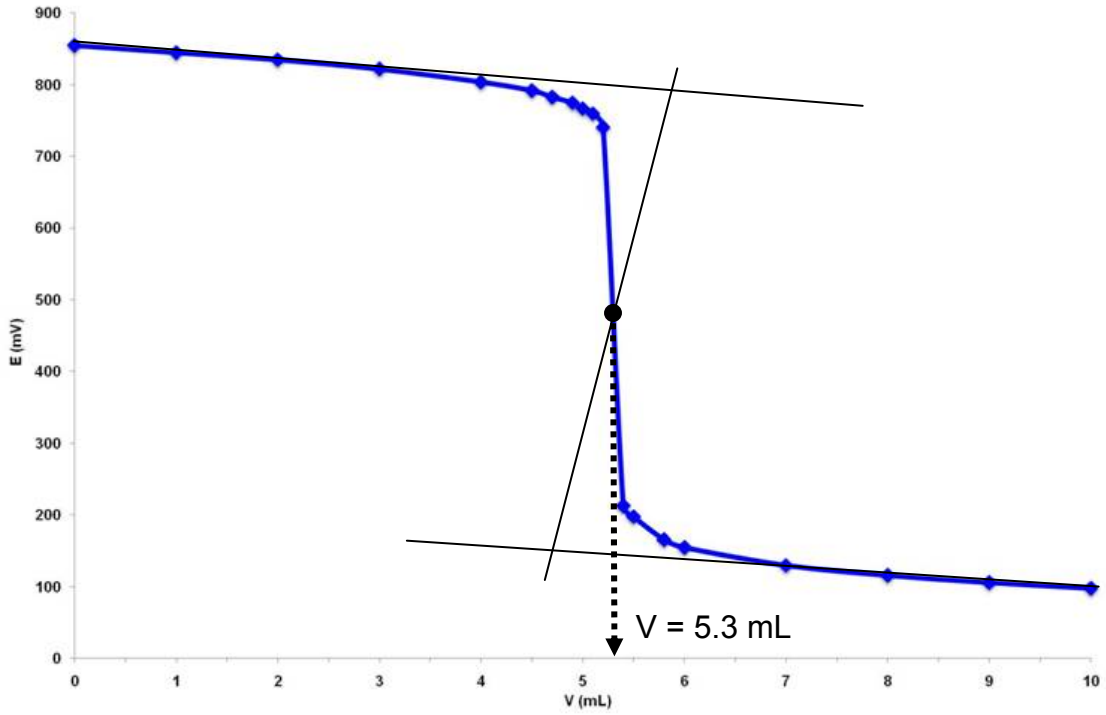

Figure S1: Potentiometric titration of **2**.

4. NMR measurements

4.1 ^{125}Te relaxation times measurements

The T_1 measurements related to the four ^{125}Te resonances observed in the ^{125}NMR spectrum of **2** were determined by a saturation-recovery experiment. The plot of the relative intensity decay as a function of time is shown in Figure S2. The T_1 relaxation times were obtained from the intensity decay equation (1). The T_2* relaxation times were calculated from the linewidths. NMR data for **2** are given in Table S3.

$$\frac{I}{I_0} = 1 - \exp\left(-\frac{t}{T_1}\right) \qquad (1)$$

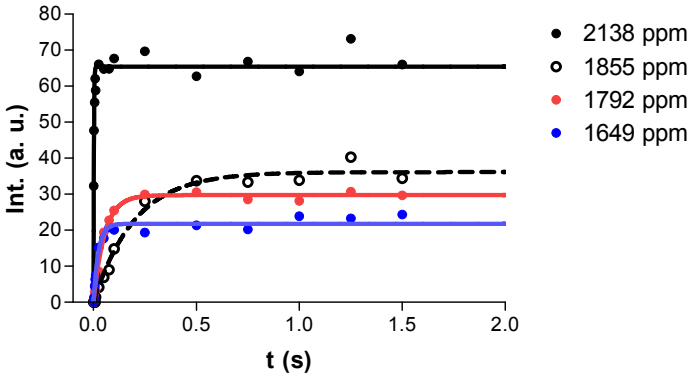

Figure S2: Intensities decay versus time delay related to the saturation-recovery experiment.

Table S3: NMR data for **2**.

line	δ / ppm	$\Delta\nu_{1/2}$	T_2* (ms)	T_1 (ms)
1	1649	22	14.5	24
2	1792	13	24.5	54
3	1855	32	63	200
4	2138	335	0.95	1.9

4.2 ^{125}Te variable temperature experiment

The ^{125}Te variable temperature NMR spectra of **2** are shown in Figure S3 and the variation of the chemical shifts is graphically shown in Figure S4.

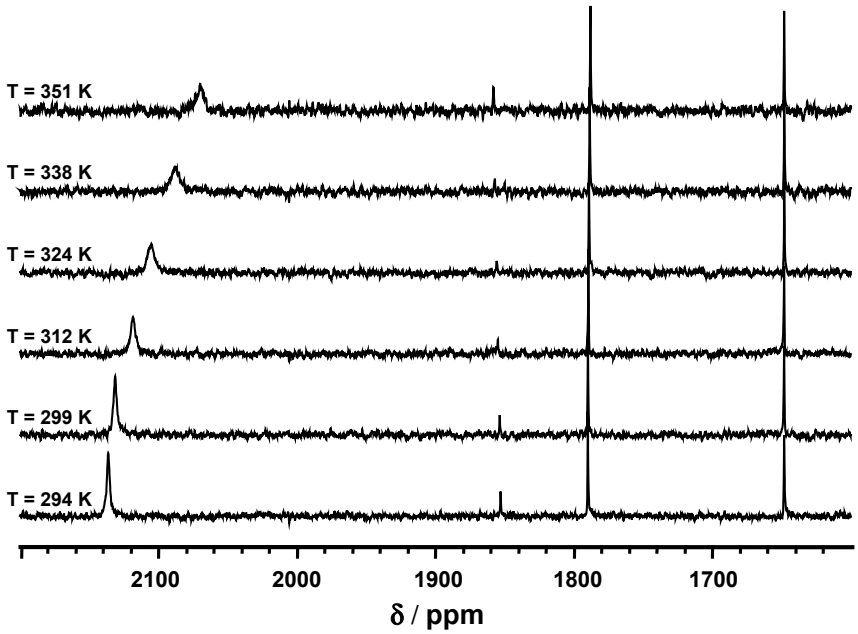

Figure S3: ^{125}Te variable temperature NMR spectra of **2**.

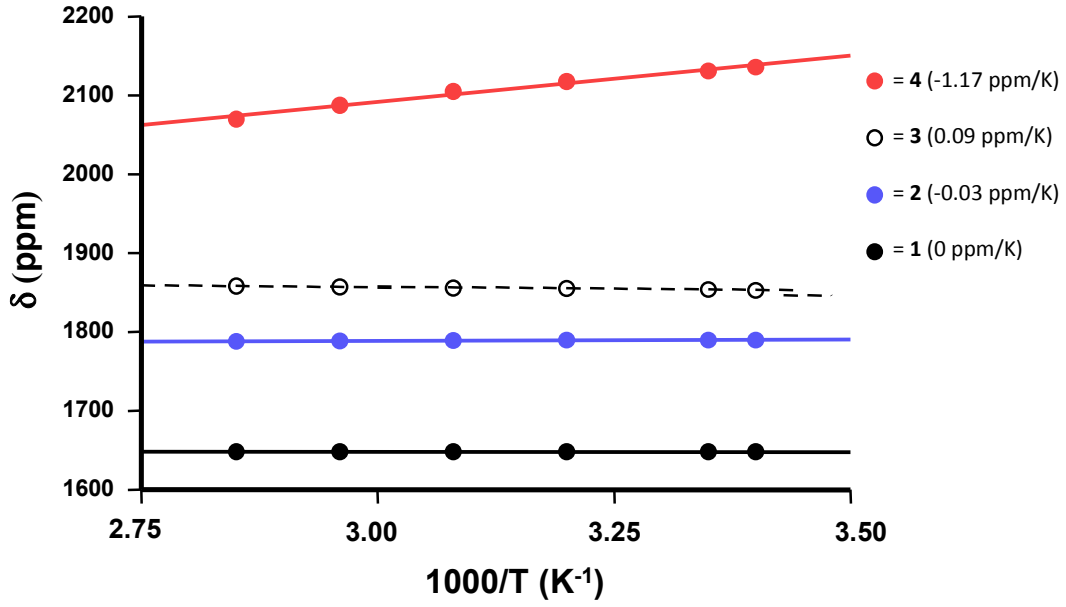

Figure S4: ^{125}Te NMR chemical shifts versus 1/T.

4.3 ^{125}Te NMR spectrum of 1

The ^{125}Te NMR spectrum of 1, shown in Figure S5 reveals the three resonance related to the presence of the anion $[Te_5Mo_{15}O_{57}]^{8-}$ at 2235, 1789 and 1647 ppm. The 1852 ppm line was attributed to the uncoordinated $[TeO_3]^{2-}$ ion and the two additional weak signals (1808 and 1803 ppm) could be tentatively assigned to encapsulated $[TeO_3]^{2-}$ species within the $\{Mo_{132}\}$ Keplerate ion.

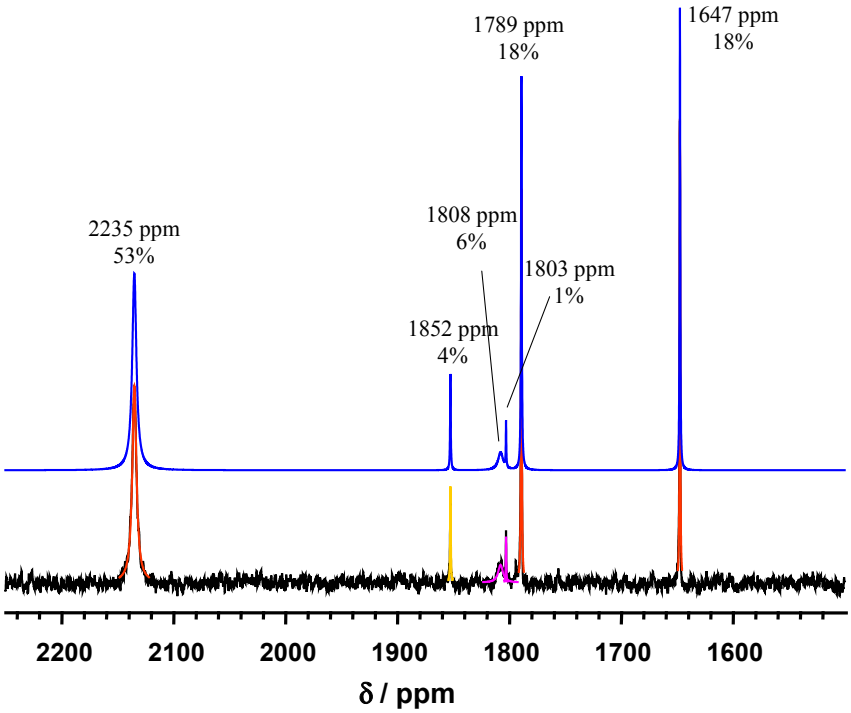

Figure S5: ^{125}Te NMR spectrum of **1**. The chemical shifts and the intensity ratios are given at the top of each line.

4.4 ^{1}H NMR spectrum of 1

The ^{1}H NMR spectrum of **1** is shown in Figure S6 and gives the ratio between the acetate ligands coordinated to the $\{Mo_2O_4\}$ linkers within the Keplerate capsule (~0.4ppm) and the uncoordinated acetate (~2ppm) according to previous works (ref. 12)

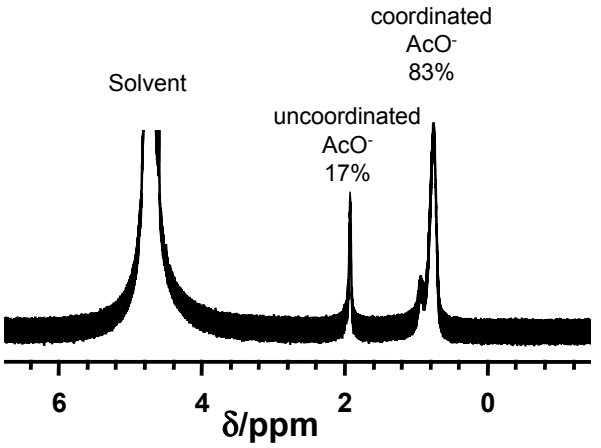

Figure S6: ^{1}H NMR spectrum of **1** showing the distribution between the coordinated and uncoordinated acetate.

5. UV-visible characterizations

5.1 Formation of the $[Te_5Mo_{15}O_{57}]^{8-}$ anion

Conversion of the $\{Mo_{132}\}$ Keplerate into the $[Te_5Mo_{15}O_{57}]^{8-}$ ion was studied at 70°C by UV-vis. $\{Mo_{132}\}$ (0.75 g; 0.157 mmol) and Na_2TeO_3 (0.255g; 6.92 mmol) are dissolved in 50 mL of water heated at 70°C. UV-vis samples were prepared from 0.2 mL samples diluted in 5 mL of water at different interval time (10 min or 30 min) and spectra recorded from 0.1cm quartz cells. The UV-vis spectra shown in Figure S7a reveal the decrease in the absorption at 450 nm related to the presence of the Keplerate ion for the benefit of absorptions above 570 nm characteristic the $[Te_5Mo_{15}O_{57}]^{8-}$ heteropolyblue.

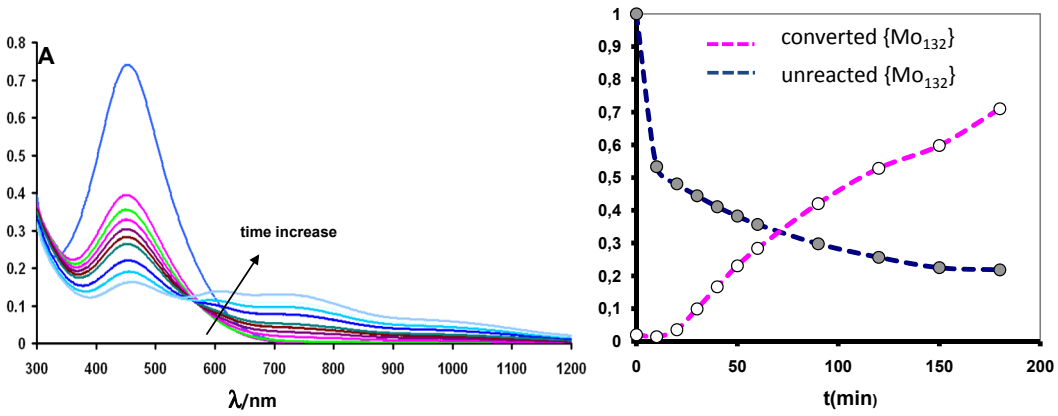

Figure S7: a) Time dependence of UV-visible spectra showing the conversion of the Keplerate anion in the presence of 44 equivalent of $[TeO_3]^{-2}$ ion. b) fraction of the unreacted and converted $\{Mo_{132}\}$ into the $[Te_5Mo_{15}O_{57}]^{8-}$ ion.

From the molar absorption coefficient ε's of both compounds (360000 $mol^{-1}L.cm^{-1}$ for $\{Mo_{132}\}$ at 450 nm and 10120 $mol^{-1}L.cm^{-1}$ at 725nm for $[Te_5Mo_{15}O_{57}]^{8-}$), the proportion of unreacted Keplerate and converted Keplerate can be calculated and plotted versus time in Figure S7b. After a short induction period (about 10 min), the proportion of the $[Te_5Mo_{15}O_{57}]^{8-}$ grows gradually. After 180 min, the sum of the fraction of unreacted and converted $\{Mo_{132}\}$ fall near 1 in agreement with a quite quantitative reaction.

5.2 Determination of the molar extinction coefficients (ε's) of the $[Te_5Mo_{15}O_{57}]^{8-}$ anion

The absorptions at 950, 725 and 610 nm versus the $[Te_5Mo_{15}O_{57}]^{8-}$ concentration are shown in Figure S8, allowing to determine the corresponding molar coefficient extinctions (8900, 10120 and 5210 $M^{-1}cm^{-1}$, respectively).

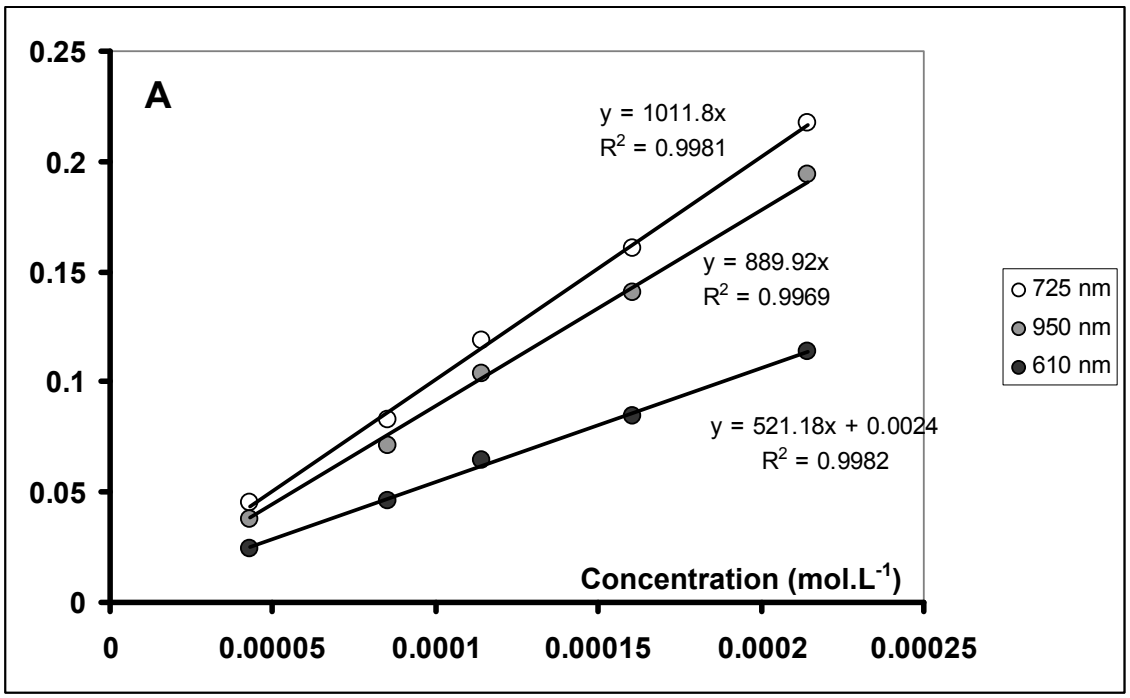

Figure S8: linear dependance of the absorbance versus concentration of $[Te_5Mo_{15}O_{57}]^{8-}$ (0.1 cm quartz cell).

6. Infrared and Raman spectroscopies

6.1 Vibrational spectra of 2b

The infrared and Raman spectra of **2b** are shown in Figure S9 and S10, respectively. The main vibrational features are given in Table S4.

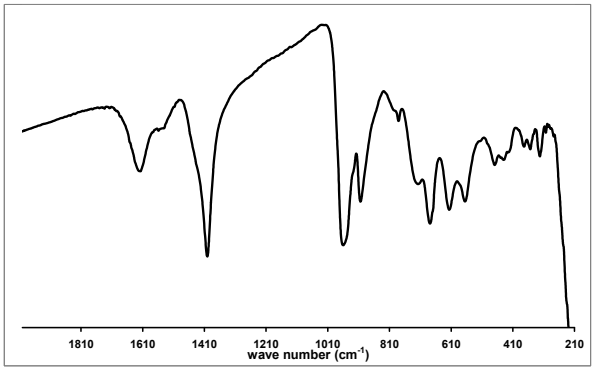

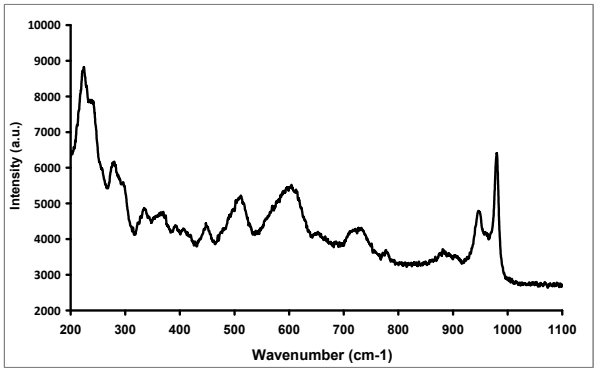

.

Table S4: Vibrational data (IR and Raman) for **2b**.

	ν(cm^{-1})			
	ν(Mo=O)	ν(Mo-O-Mo)	ν(Mo-O-X) X=Mo or Te	non attributed
infrared	959(s) 903(m)	781(vw)	719(m) 678(s)	616(m), 561(m), 467(w), 438(w), 428(w)
Raman	980(s) 961(sh) 947(m)	905(w) 888(w) 778(vw)	732(w) 715(w) 654(w)	604(m), 511(m), 450(w), 409(w), 394(vw), 367(w), 336(w), 297(w), 280(m), 240(m), 224(s)

Figure S9: Infrared spectrum of **2b**.

Figure S10: Raman spectrum of **2b** (solution).

6.2 Vibrational spectra of 1

Infrared and Raman spectra of **1** compared with that of the Keplerate {Mo_{132}} anion are shown in Figures S11 and S12 respectively. The main differences observed in the IR spectrum of **1** lie in the presence of a weak absorption at 904 cm^{-1} and a shoulder at 688 cm^{-1}, both characteristic of the presence of the $[Te_5Mo_{15}O_{57}]^{8-}$ anion, while no significant difference was observed in the Raman spectrum of **1** and **2.** The vibrational features of **1** are given in Table S5.

Table S5: vibrational features (IR and Raman) of **1**.

	ν(cm^{-1})			
	ν(Mo=O)	ν(Mo-O-Mo)	ν(Mo-O-X) X=Mo or Te	non attributed
infrared	966(s) 936(sh) 903(vw)	857(m) 794(s) 725(s)	680(sh)	626(w), 569(m), 514(vw), 468(vw), 419(vw)
Raman	964(w) 950(w)	882(s) 851(sh)		755(vw), 714(vw), 374(m), 313(w), 218(vw)

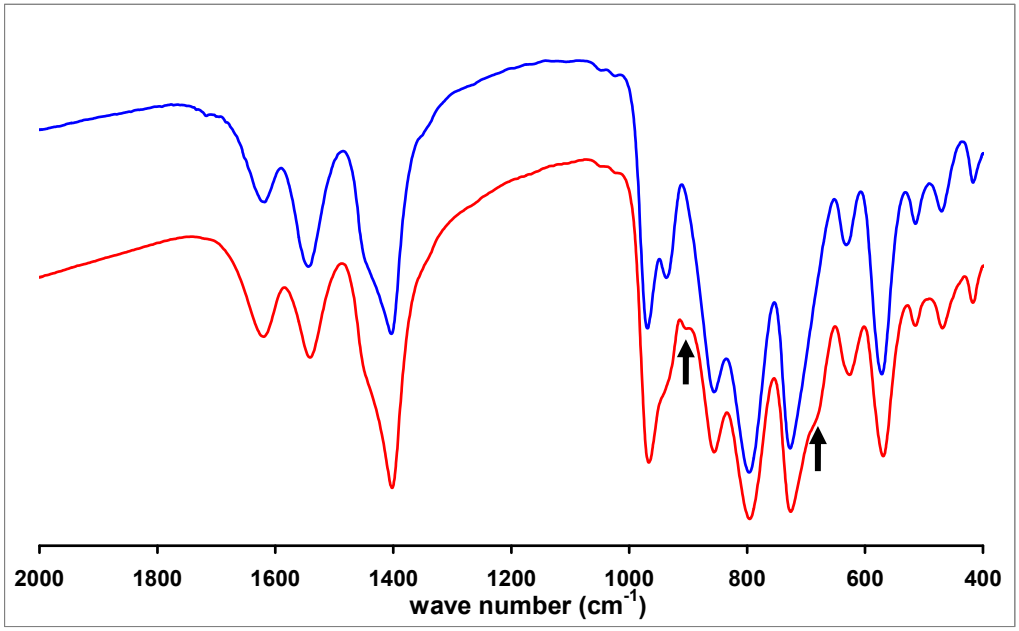

Figure S11: Infrared spectrum of **1** (red) compared with that of {Mo_{132}} Keplerate (blue). The main differences are indicated by arrows and correspond to contributions of the $[Te_5Mo_{15}O_{57}]^{8-}$ anion.

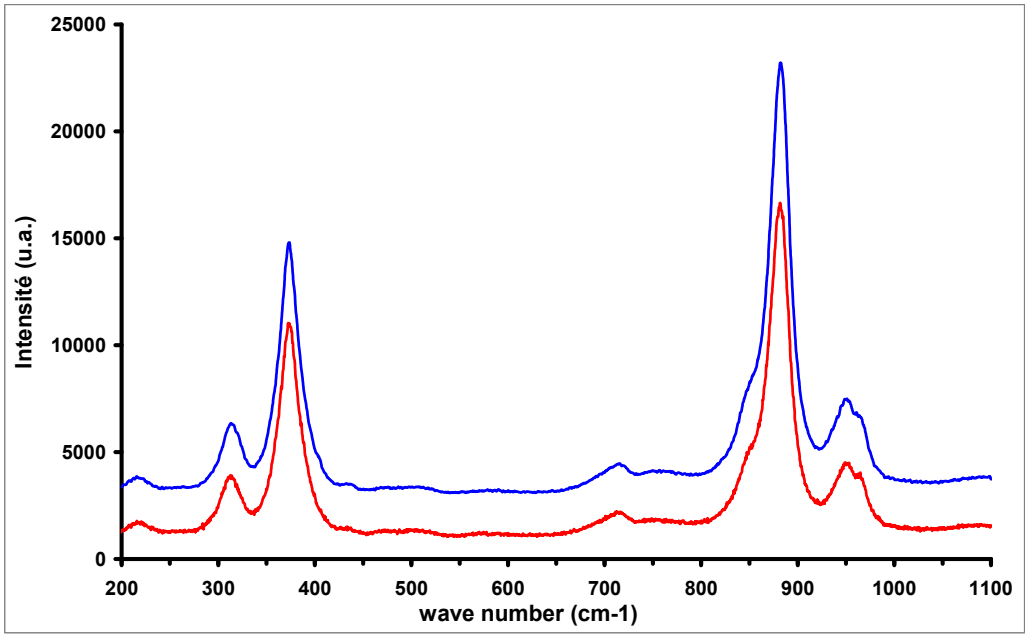

Figure S12: Raman spectrum of **1** (red) compared with that of {Mo_{132}} Keplerate (blue). No significant difference was observed.

7. XRD diagram of the $Mo_{8.22}V_{1.78}Te_{0.79}O_{29}\bullet 1H_2O$ (M1 phase)

The X-ray diffraction pattern of the multielement MoVTe oxide phase is shown in Figure S13 and exhibit the most intense diffraction peaks at 2θ = 6.7, 7.9, 9.1, 10.9, 13.1, 22.3, 26.2, 26.7, 27.3, 28.2, 29.2, 30.5, 31.3 and 35.5°. The calculated X-ray diffraction pattern has been obtained from the crystal data provided in ref. [3] (Orthorhombic, space group Pba2, a = 21.134 Å, b = 26.658 Å , c = 4.0146 Å)

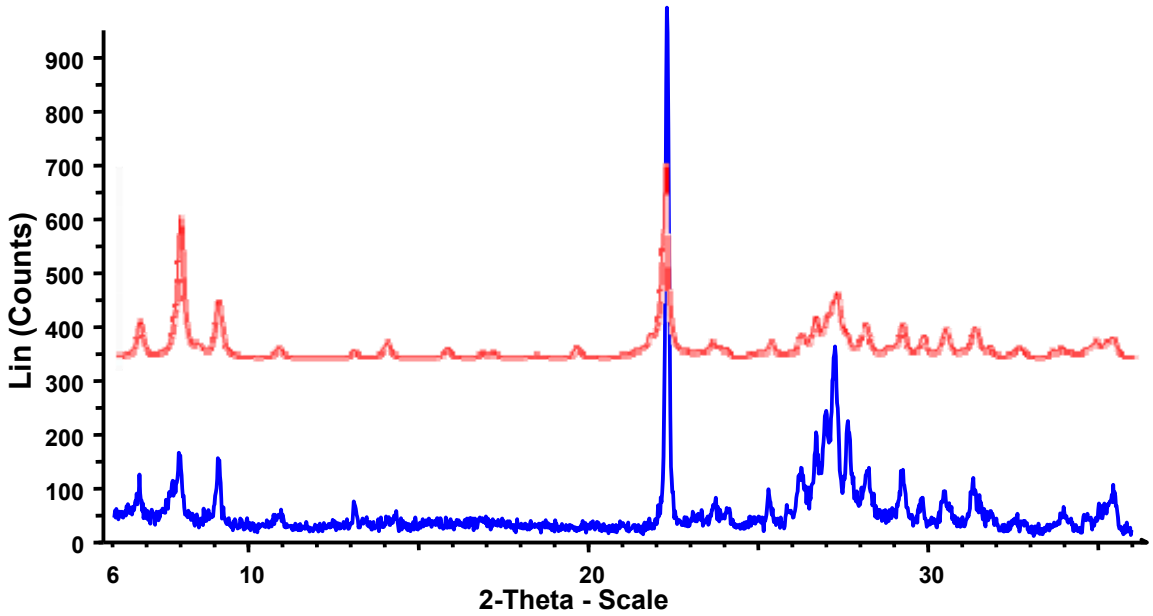

Figure S13: X-ray powder diagram of $Mo_{8.22}V_{1.78}Te_{0.79}O_{29}\bullet 1H_2O$ (M1 phase) (blue), compared to that calculated from the X-ray crystal data (red).

8. DFT calculations

8.1 Optimized geometry of the anion 2b

All the DFT calculations have been performed using the AFD package (1). The molecular orbitals are developed on triple zeta plus polarization atomic orbital. The core electron (up to 4p for Te, 3d for Mo and 1s for O) are frozen numerical. The energy is computed using the PBE functional (2).

Full geometrical optimizations have been carried out following 2 methods. In a first step, the POM structure with three ammonium molecules has been optimized in vacuum. The computed Mo-Te distances were 30% larger than the crystallographic ones. The effect of the hydrogen bond between the $\{TeMo_6O_{24}\}$ and the $\{TeMo_9O_{33}\}$ subunits is very large. Indeed a vacuum optimization with the ammonium cations leads to the destruction of the structure.

In a second step, solvent effects have been added in the optimization using the Cosmo (3) method. The computed distances, compared with the corresponding experimental ones are given in Table S6. The calculated values appear quite similar to the crystallographic ones differing by an average error of about 4% (see Table S6). The numbering of the Mo, O and Te atoms within the C_{3v} optimized $[Te_5Mo_{15}O_{57}]^{8-}$ anion are shown in Figure S14.

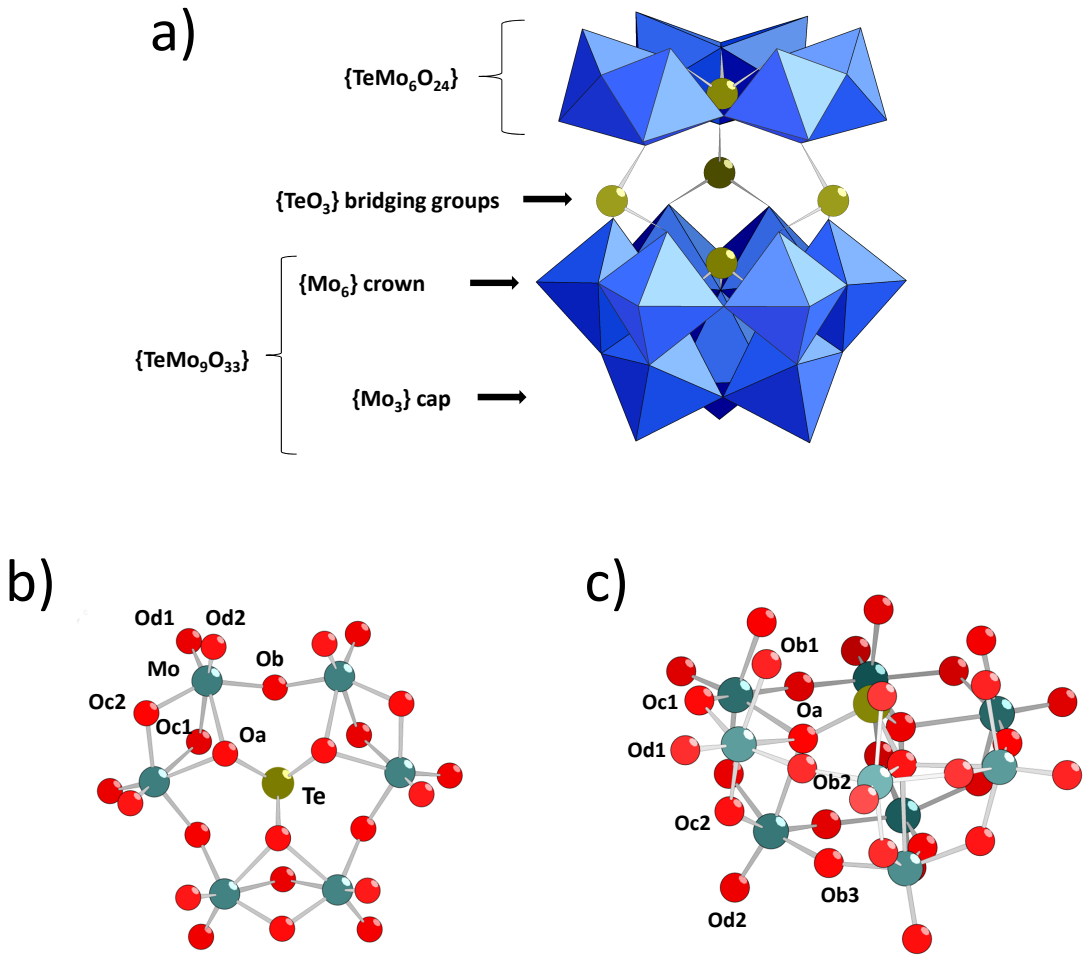

Figure S14 : Representation and labelling of the anion **2** with the idealized C_{3v} symmetry. a) the anion **2** consists of the two structural subunits $\{TeMo_6O_{24}\}$ and $\{TeMo_9O_{33}\}$ bridged by three Te atoms. Labelling of the oxygen atoms within b) $\{TeMo_6O_{24}\}$ and c) $\{TeMo_9O_{33}\}$.

Table S6 : Computed and experimental bond distances within $[Te_5Mo_{15}O_{57}]^{8-}$ anion (C_{3v} optimized symmetry)

	$\{Mo_6O_{24}\}$ capping-crown						
	Mo-Oa	Mo-Ob	Mo-Oc1	Mo-Oc2	Mo-Od1	Mo-Od2	Te-Oa
Calc.	2.23	2.00	2.57	2.02	1.76	1.75	1.97
Exp.	2.19	1.94	2.30	1.98	1.73	1.71	1.87
	$\{TeO_3\}$ bridging groups						
	Te-Oc1	Te-Ob1					
Calc.	1.92	1.97					
Exp.	1.82	1.90					
	$\{TeMo_9O_{33}\}$ subunit						
	$\{Mo_6\}$ crown						
	Mo-Oa	Mo-Ob1	Mo-Ob2	Mo-Oc1	Mo-Oc2	Mo-Od1	Te-Oa
Calc.	2.42	2.09	1.95	2.05	1.90	1.74	1.92
Exp.	2.38	2.04	1.89	2.00	1.88	1.69	1.87
	$\{Mo_3\}$ cap						
	Mo-Oa	Mo-Ob3	Mo-Oc2	Mo-Od2			
Calc.	2.57	1.95	2.00	1.73			
Exp.	2.47	1.90	1.95	1.68			

8.2 Te NMR chemical shifts calculation.

In order to strengthen the Te-NMR assignment, Te chemical shifts have been calculated (4) for both optimized structures (vacuum and solvent). The computed chemical shifts are found to reproduce the experimental order between the three ^{125}Te chemical shifts (see Table S7).

Table S7 : computed ^{125}Te NMR chemical shifts of $[Te_5Mo_{15}O_{57}]^{8-}$

		Bridging $\{TeO_3\}$	**$\{TeMo_6O_{24}\}$**	**$\{TeMo_9O_{33}\}$**
$\delta(^{125}Te)$/ppm		2138	1792	1649
$\Delta\delta$ / ppm	Exp.		+346	+143
	Calc.		+400[a](+540)[b]	+50[a](+50)[a]

calculated in vacuum[a] and in solvent[b]

(1) www.scm.com.

(2) J. P. Perdew, K. Burke and M. Ernzerhof, *Generalized Gradient Approximation Made Simple.* Physical Review Letters **77**, 3865 (1996).

(3) A. Klamt and G. Schüürmann, *COSMO: a new approach to dielectric screening in solvents with explicit expressions for the screening energy and its gradient.* Journal of the Chemical Society: Perkin Transactions **2**, 799 (1993).

(4) G. Schreckenbach and T. Ziegler, *The calculation of NMR shielding tensors using GIAO's and modern density functional theory.* Journal of Physical Chemistry **99**, 606 (1995).